Journal of Materials Research and Technology 29 (2024) 3237–3248

Contents lists available at ScienceDirect

Journal of Materials Research and Technology

journal homepage: www.elsevier.com/locate/jmrt

Enhancing efficiency and sustainability of digital light processing 3D-Printing by novel two-stage processing of carbon nanotube reinforced nanocomposites

A. Cortés [a,*], M. Bañón-Veracruz [b], A. Jiménez-Suárez [a], M. Campo [a], M.G. Prolongo [b], S.G. Prolongo [a,c]

[a] Materials Science and Engineering Area, Escuela Superior de Ciencias Experimentales y Tecnología, Rey Juan Carlos University, Calle Tulipán s/n, 28933, Móstoles, Madrid, Spain
[b] Department of Aerospace Materials and Processes, Escuela Técnica Superior de Ingeniería Aeronáutica y del Espacio, Polytechnic University of Madrid, Plaza Del Cardenal Cisneros 3, 28040, Madrid, Spain
[c] Instituto de Tecnologías Para la Sostenibilidad, University Rey Juan Carlos, C/Tulipán s/n, 28933, Móstoles, Madrid, Spain

ARTICLE INFO

Handling Editor: SN Monteiro

Keywords:
Additive manufacturing
3D printing
Nano composites
Carbon nanotubes
Smart materials
Two-stage processing

ABSTRACT

3D printing has gained a spot within the industry during the last decade due to the advantages it presents regarding conventional manufacturing technologies. Nevertheless, the high processing time and the material waste due to the use of printing supports are still some of the main challenges that have to be addressed. In this research work, a simple strategy to minimize the processing time and the material waste is carried out through a two-stage processing method. Here, a flat specimen is obtained using a vat photopolymerization 3D printer, presenting a low curing degree. Then, the specimen is bent and subsequent post-curing treatments are performed to increase the cross-link density, thus fixing the desired shape. Furthermore, carbon nanotubes were used as nanoreinforcement for increasing the mechanical properties and exploiting their Joule heating capabilities for the thermal post-curing treatment, being way less energy-consuming (around 1W) than using a conventional oven (around 750 W). The results obtained with a proof-of-concept evinced the suitability of the proposed two-stage processing method to enhance the efficiency and sustainability of the 3D printing process. The printing time and the material waste were reduced by 94.3 % and 16.7 % on average, respectively, with regard to printing the part directly on its final desired shape, as well as showing a shape fixity ratio of around 98 %. Furthermore, an enhancement of the mechanical properties was obtained due to the reorientation of the printed layers during the two-stage processing.

1. Introduction

During the last decade, 3D printing has proven to be a true alternative to conventional manufacturing techniques due to the advantages it presents within the framework of Industry 4.0 [1–3]. One of them is the capability of obtaining custom or even unique parts without significantly increasing the manufacturing cost [4,5]. Other advantages regarding conventional manufacturing techniques are the possibility of obtaining complex geometry parts in one single piece without joints or assemblies, the low upfront investment, the fast product development through rapid prototyping, and the shortening of the supply chain, among others [6–8].

In this context, new business models based on 3D printing, such as printer farms, have emerged, where several 3D printers work in parallel [9]. Here, the limiting factor to increase the production volume is often the printing time [10], since the nature of additive manufacturing is to obtain, layer by layer, the desired geometry from a 3D model. On the other hand, complex geometry parts often need the use of supports during printing, depending mainly on the angle with respect to the printing platform and the length of the overhangs [11], which results in longer lead times to obtain the final product due to the extra time needed for removing the supports and polishing the support-part contact zone for a better surface finish [12]. In this regard, reducing the need for using supports is especially important for 3D printing technologies using

* Corresponding author.
E-mail address: alejandro.cortes@urjc.es (A. Cortés).

https://doi.org/10.1016/j.jmrt.2024.02.018
Received 21 November 2023; Received in revised form 15 January 2024; Accepted 3 February 2024
Available online 13 February 2024

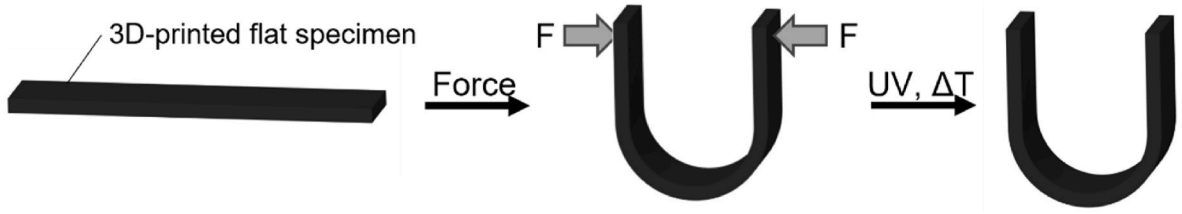

Fig. 1. Scheme of the proposed method for fixing the final shape by simply applying a force and performing subsequent UV and thermal post-curing stages.

Table 1
Gap distance between rolls during the calendering process.

Gap 1 (μm)	Gap 2 (μm)	Number of Cycles
120	40	1
60	20	1
45	15	1
15	5	4

thermoset resins, as Vat Photopolymerization, since the recyclability of the material used in the supports is quite limited [13].

The present research work aims to improve the efficiency and sustainability of the 3D printing process through the minimization of the printing time and material waste during 3D printing by performing the so-called two-stage processing. This method consists of first obtaining an intermediate shape with a cross-link density and glass transition temperature (T_g) low enough to be conformed into a different geometry and then fixing that desired shape by carrying out a second curing stage, thus increasing the cross-link density [14]. As schematized in Fig. 1, flat specimens, which require a low printing time and eliminate the possibility of requiring support material, are manufactured using a Digital Light Processing (DLP) 3D printer, obtaining a partially cured specimen, i.e., over the gel time but below its maximum cross-link density. Then, a force is swiftly applied to bend them into the desired shape to perform subsequent ultraviolet (UV) and thermal post-curing stages for fixing the final shape by completing the curing process of the specimens in the desired shape. It is worth mentioning that the process could be fully automated to obtain complex and/or custom geometries.

In this regard, it is possible to save printing time, as the number of printing layers can be considerably lower than directly printing the part on its final shape, improving the efficiency of the 3D printing process. Moreover, as printing the specimens flat does not require the use of printing supports, depending on the final desired geometry, it is possible to reduce the material waste due to eliminating the need for these supports when printing the part directly on its final desired shape, which promotes sustainability [15].

The key to time and material waste reduction is that both the conventional and two-stage processing approaches need the post-curing stages to reach the final properties of the part. In this context, the time used for applying a force to the specimen in the two-stage processing method could be similar to the time needed for removing the printing supports of conventional 3D printing. Thus, the two-stage processing can be considerably faster than the conventional 3D printing method due to printing flat specimens, which requires printing fewer layers without using support structures.

Some interesting research studies found in the literature develop 3D printable formulations with dual-curing capabilities for different purposes, such as the enhancement of mechanical properties [16], self-healing/repairability [17], or in-situ generation of silver nanoparticles [18]. Nevertheless, as far as the authors know, no research works have been published about using the aforementioned dual-curing capabilities of 3D printable formulations to reduce material waste due to the usage of printing supports and just one research work has been reported about using this processing technique to reduce printing time

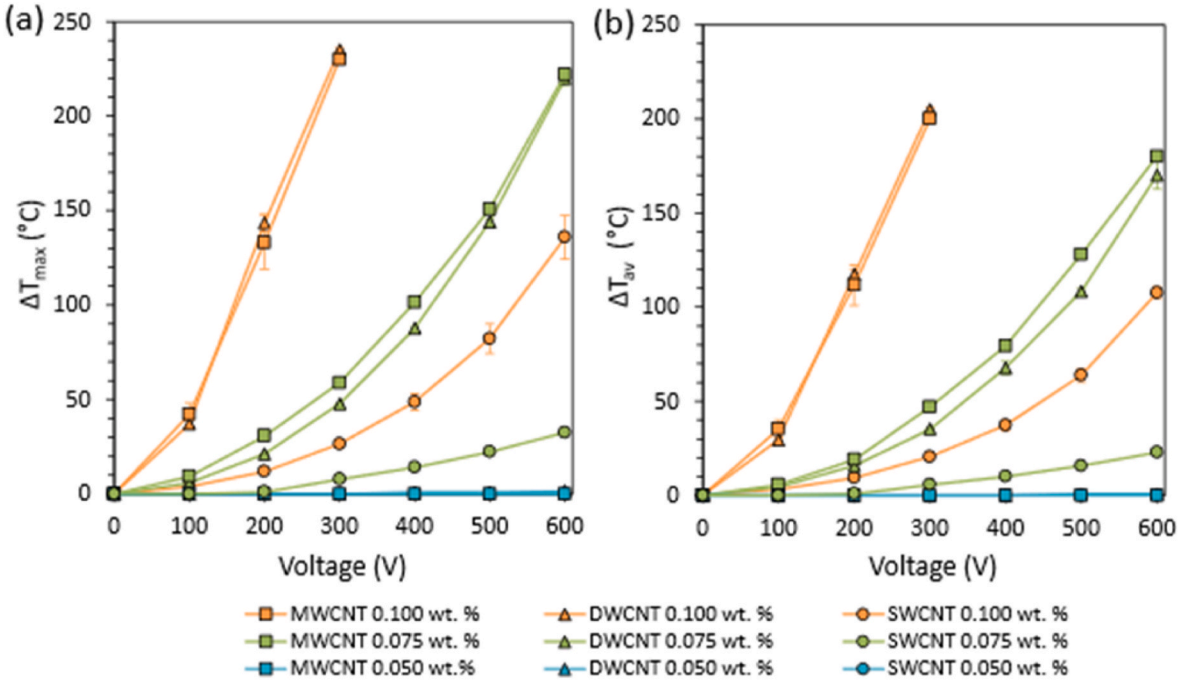

Fig. 2. Thermoelectrical characterization. Maximum (a) and average (b) temperature increment (ΔT_{max} and ΔT_{av}, respectively) with regard to room temperature as a function of the applied voltage, CNT type, and CNT content.

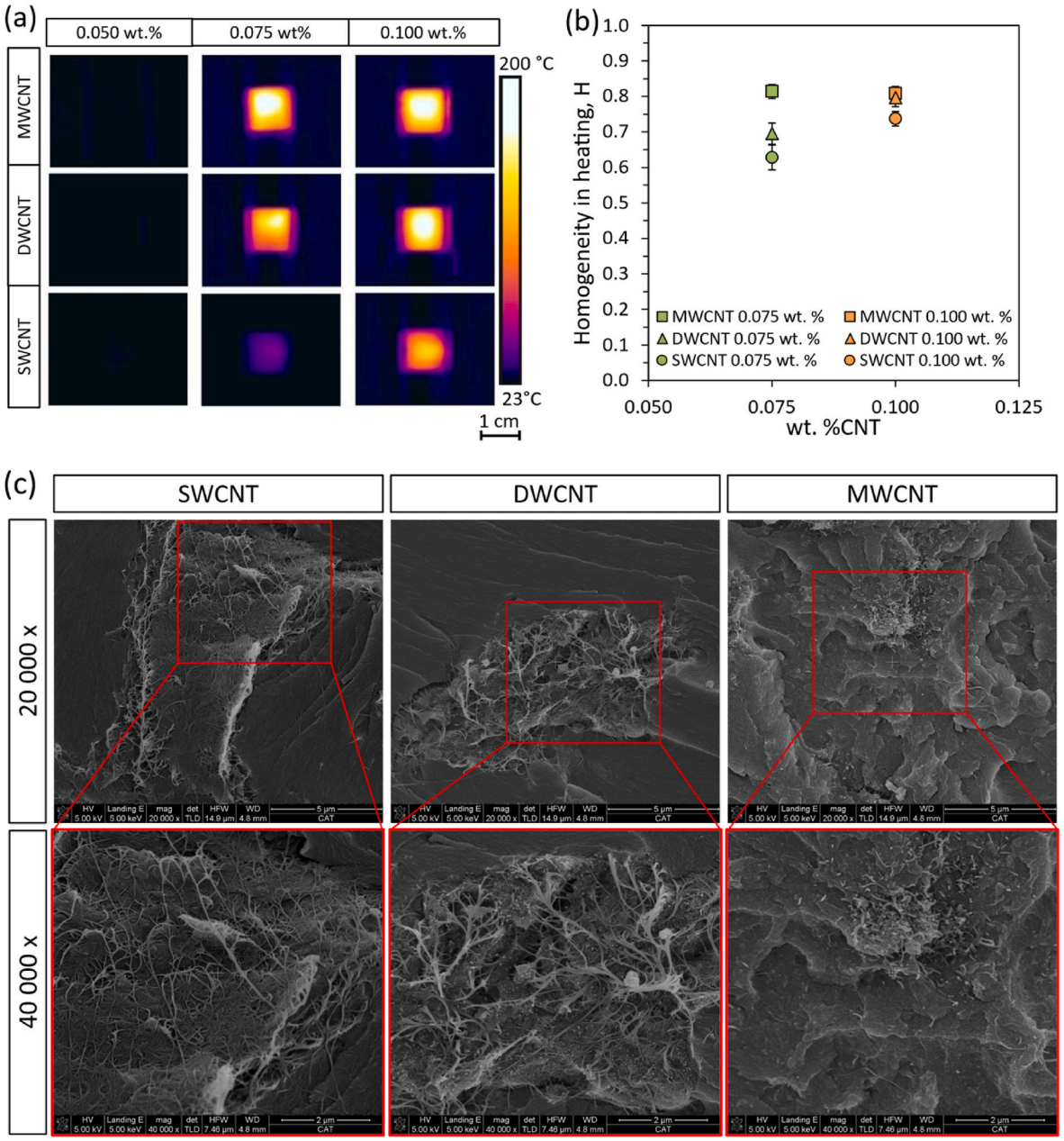

Fig. 3. (a) Thermographs of the maximum temperature reached during the thermoelectrical characterization tests, (b) homogeneity in heating, as a function of the CNT type and content, and (c) FEG-SEM micrographs of the nanocomposites containing 0.075 wt% of SWCNT, DWCNT, and MWCNTs, respectively.

[19]. Nevertheless, the exact reduction of printing time was not reported. In this context, it is important to shed light on this topic to push the boundaries of advanced manufacturing.

On the other hand, the use in the present study of carbon-based nanoparticles, like carbon nanotubes (CNTs), as reinforcement in the developed materials, allows not only to increase the mechanical properties caused by the effective reinforcement of the nanoparticles [20–23] but also to reduce energy consumption during the thermal post-curing stages. This is possible due to the Joule heating capabilities of these nanocomposites when an electrical current flows through the material [24,25]. In this context, the Joule heating is released inside-out of the specimen whereas a conventional oven works oppositely because of the nature of convection heating, being the latter one way less efficient and more expensive.

Furthermore, a hook-like geometry was proposed in this study as a proof-of-concept, which can be used underwater. Since one of the main drawbacks of thermosetting polymers is the loss of mechanical properties and dimensional stability [26,27], the effect of the CNTs on hydrothermal aging was studied in this research work. In this context, there are few research works studying the hydrothermal aging of acrylate-based formulations for additive manufacturing [28,29]. Nevertheless, these works are mainly focused just on dental applications, where no nanoreinforcement was used to minimize the negative effects of hydrothermal aging. In this research work, the use of a highly crosslinked formulation, together with the use of CNTs, seeks to minimize the aforementioned negative effects of hydrothermal aging.

2. Materials and methods

2.1. Materials

The nanocomposites developed in this study are based on a

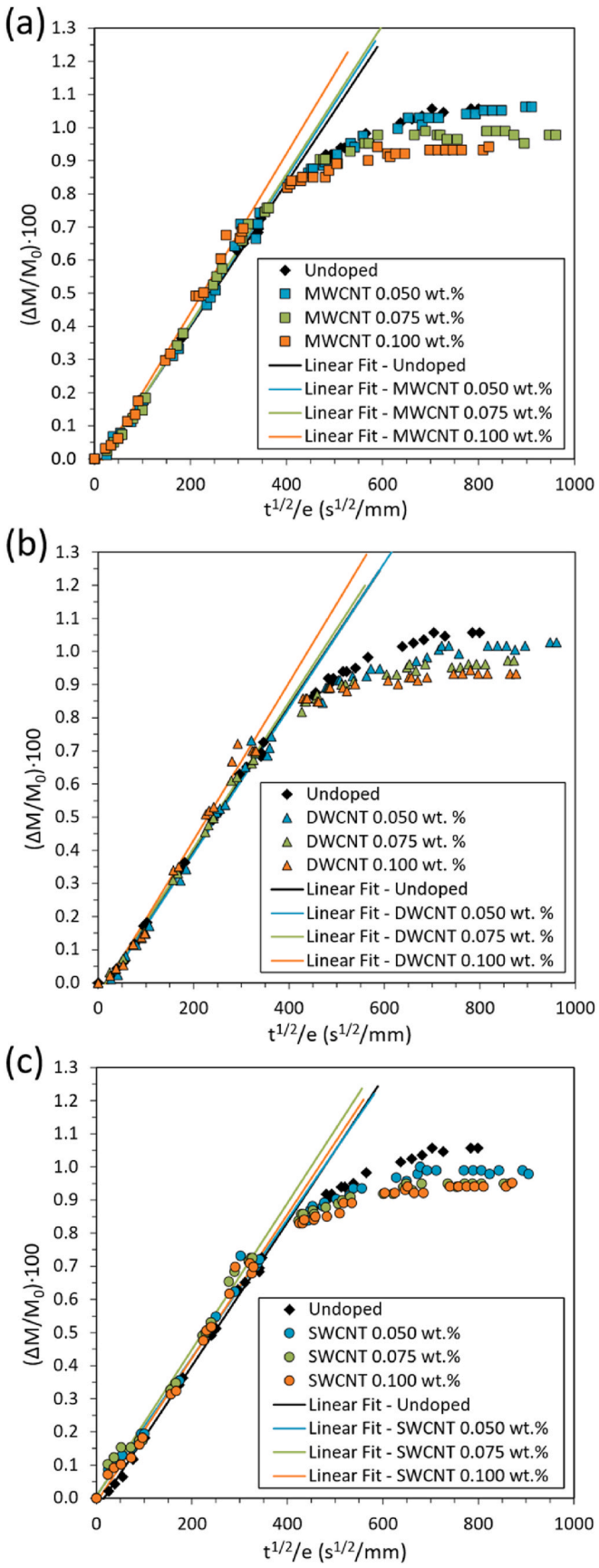

Fig. 4. Water uptake as a function of time and content for (a) MWCNT, (b) DWCNT, and (c) SWCNT doped nanocomposites.

commercial resin, High Temp Resin v2 supplied by Formlabs, which is based on acrylated monomers and methacrylated oligomers. This resin was doped with three different types of carbon nanotubes, which were added to the matrix in three different contents: 0.050, 0.075, and 0.100 wt %. The first ones are single-wall carbon nanotubes with 3.96 wt% OH content from Cheaptubes, which present a length between 10 and 30 μm and a diameter of 1–2 nm. The second ones are HDPlas single-wall/double-wall carbon nanotubes from Cheaptubes, with a length between 3 and 30 μm and a diameter of 1–2 nm. Finally, the third ones are multi-wall carbon nanotubes NC7000 from Nanocyl, which present an average length and diameter of 1.5 μm and 9.5 nm, respectively. From here on, the abbreviations used in this paper for the carbon nanotubes used for this study are SWCNTs, DWCNTs, and MWCNTs, respectively.

2.2. Manufacturing

First, a calendering process was carried out to disperse the CNTs into the matrix, following a previously optimized 7-step procedure [30], where the distance between rolls was reduced each step (Table 1).

Then, the dispersion is ready to be used in the 3D printer equipment, a B9Creator by B9Creations, which uses Digital Light Processing (DLP) technology. Here, a high-definition digital projector illuminates the resin vat, layer by layer, with cross-sectional images of the 3D model [31]. The main printing parameters used in this study are a light exposure time of 5.12 s and a layer thickness of 30 μm for all specimens, which were optimized in a previously published research work [32].

2.3. Thermoelectrical characterization

The thermoelectrical characterization was carried out by analyzing the temperature reached by the Joule effect, using the FLIR E50 thermal camera from FLIR Instruments, as a function of the applied voltage with a Keithley 2410 power source from Keithley Instruments. The average and maximum temperature increments (ΔT_{av} and ΔT_{max}, respectively) with regard to room temperature (around 23 °C) were analyzed with FLIR Tools + software on 1 × 1 × 0.1 cm^3 specimens. Here, copper electrodes were attached to the specimens by using silver conductive paint on two opposite 1 × 0.1 cm^2 faces of the specimens to reduce contact resistance. Furthermore, the homogeneity in heating, H, was calculated from equation (1):

$$H = 1 - (\Delta T_{max} - \Delta T_{av}) / \Delta T_{max} \quad (1)$$

2.4. Water uptake characterization

Once printed, the 35 × 12.7 × 1.4 mm^3 samples were immersed in distilled water at 40 °C and weighed over time to determine the amount of water absorbed, thus studying its diffusion kinetics. The diffusion coefficient, D, is obtained from equation (2):

$$D = \left[\frac{m}{4 \cdot M_\infty}\right]^2 \pi \cdot \beta \quad (2)$$

where m is the slope of the curve resulting from representing the increase in relative weight, $\Delta M/M_0$, against $t^{1/2}/e$ (where e is the thickness of the sample and t the time), M_∞ is the mass of the sample when it reaches the equilibrium, and β is a correction coefficient that reduces the error because diffusion occurs on all faces, that is, the sample is a three-dimensional plate. The equation used to calculate the β coefficient is:

$$\beta = 1 + \frac{e}{a} + \frac{e}{b} \quad (3)$$

where a and b are the width and length of the sample, respectively.

Moreover, the effect of the water uptake in the thermomechanical properties was characterized by means of Dynamic Mechanical Thermal Analysis (DMTA), using DMTA V equipment by Rheometric Scientific.

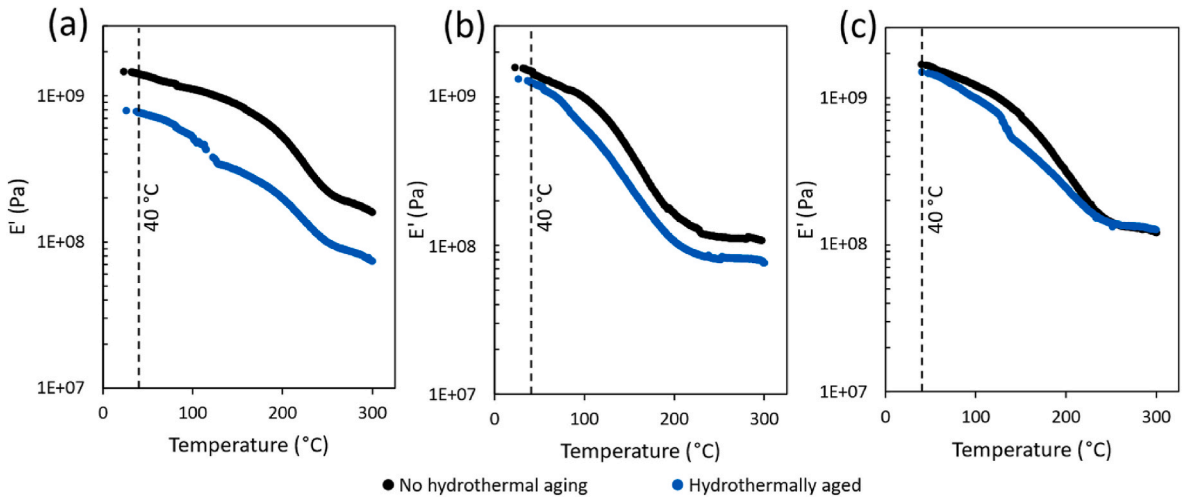

Fig. 5. Storage modulus, E′, before and after the water uptake tests obtained by DMTA carried out for (a) the undoped specimens, (b) the 0.1 wt%MWCNT reinforced nanocomposites, and (c) the 0.1 wt%DWCNT reinforced ones.

Here, the glass transition temperature, T_g, and storage modulus, E', of the specimens were evaluated before and after the water uptake tests. In this regard, the T_g of the acrylate-based networks was taken at the maximum of the tan δ-temperature curves. For this study, measurements were done in dual cantilever bending mode at 1 Hz and strain of 0.1 %, with temperature sweeps increasing from 30 to 300 °C at 2 °C/min. In addition, two sweeps per sample have been performed to adequately analyze the curing degree reached by the specimens.

2.5. Thermomechanical behavior

After the printing process was completed, different post-curing treatments were performed. The UV post-curing treatment was carried out in a UV oven, B9A-LCB-020 from B9Creations, for 30 min, whereas the thermal post-curing treatment was conducted at 200 °C for 1 h. In this sense, the thermal post-curing treatment was carried out by using 2 different heating sources: a conventional oven (Carbolite PN30) and by Joule effect, using the Keitley 2410 from Keithley power source and the FLIR E50 thermal camera to control that the average temperature of the specimen is kept at around 200 °C.

In this context, an analysis of the curing degree was carried out by DMTA, following the same conditions mentioned in the water uptake section. Here, the T_g and E' of the as-printed specimens were evaluated and compared with the ones that received UV and thermal post-curing treatments, respectively.

2.6. Shape fixity characterization

To evaluate the effectiveness of the post-curing process to fix the desired shape from the original one, a U-shaped mold was used to introduce the as-printed specimens for the subsequent UV and thermal treatments. The mold bends 180° the specimens of 50.2 × 12.7 × 1.4 mm^3 with a curvature radius of 9 mm. Then, the Shape Fixity Ratio (S_F) was evaluated by equation (4), measured by image analysis (ImageJ software) the bending angle of the specimens as a function of the curing route.

$$S_F(\%) = \left(1 - \frac{\theta_M - \theta_F}{\theta_M}\right) \cdot 100 \quad (4)$$

Here, θ_M represents the angle of the specimen when the force is being applied (180°), whereas θ_F represents the fixing angle of the specimen once the force is released after the subsequent post-curing stages. All fixing angle measurements were taken 30 min after the applied force was released to ensure that the obtained shape was stable on time.

2.7. Microscopy

A Leica DMR optical microscope equipped with a Nikon 990 camera was used to study the curved region of the specimens, whereas the dispersion of the nanoreinforcement was studied by Field Emission Gun – Scanning Electron Microscopy (FEG-SEM) using a Nova Nano-SEM FEI 230 from Philips.

3. Results and discussion

3.1. Thermoelectrical characterization

Fig. 2 shows the maximum (Fig. 2a) and average (Fig. 2b) temperature increments with regard to room temperature (ΔT_{max} and ΔT_{av}, respectively) reached by Joule heating as a function of the applied voltage, CNT type, and CNT content.

Here, an increase in the temperature reached by the Joule effect can be observed when increasing the CNT content, regardless of the CNT type. More specifically, the specimens containing 0.1 wt% DWCNTs showed the highest temperature, closely followed by the ones containing 0.1 wt% MWCNTs. This is directly related to the electrical conductivity, which was already measured in a previous study [33]. In this context, the higher the electrical conductivity (K), the lower the electrical resistance (R) and, thus, the higher the current intensity (I) for the same applied voltage (V) (see equations (5) and (6), respectively). Thus, the heat released by the Joule effect (Q) increases as it is directly proportional to the square of the current intensity, (see equation (7)).

$$K = L/(A \cdot R) \quad (5)$$

$$V = I \cdot R \quad (6)$$

$$Q = I^2 \cdot R \cdot t \quad (7)$$

Where L and A are the length and the cross-sectional area of the specimen, respectively, while t is the time.

In this same sense, the lower temperature reached by the nanocomposites containing SWCNT with regard to the DWCNT and MWCNT nanocomposites lies on the significantly lower electrical conductivity of the first ones due to the poor dispersion of the nanoreinforcement into the matrix [33].

It is important to highlight that the differences between the maximum and the average temperatures reached by Joule heating can be explained by the presence of CNT aggregates, which generate regions within the specimen with higher and lower electrical conductivity and, thus, regions that achieve higher and lower temperatures during Joule

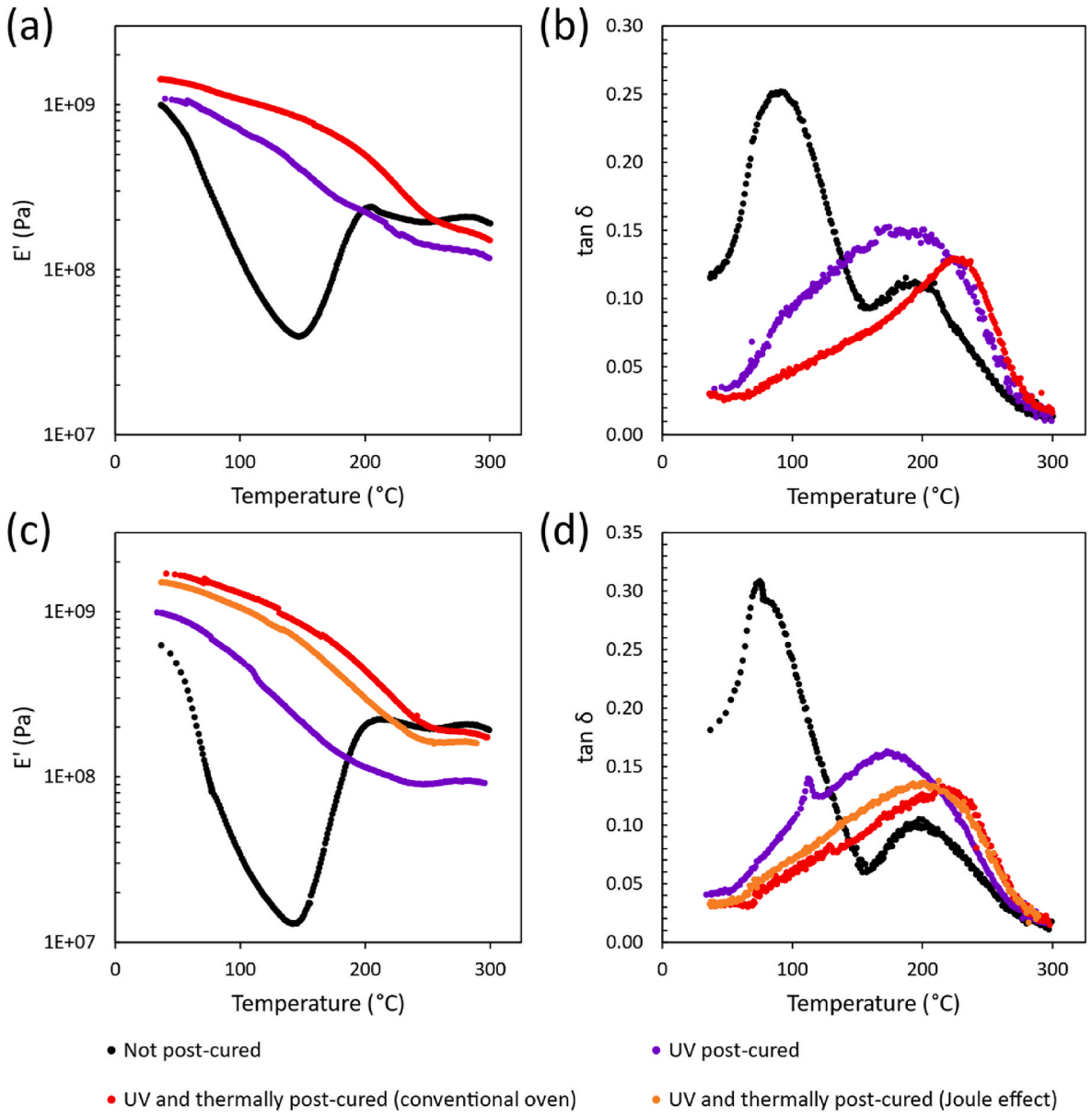

Fig. 6. DMTA curves for the undoped and CNT reinforced nanocomposites as a function of the post-curing treatment. Storage modulus and tan δ of the undoped specimens, (a) and (b), respectively. Storage modulus and tan δ of the 0.1 wt% DWCNT doped specimens, (c) and (d), respectively.

heating. Nevertheless, the outer regions of the specimen showed the lowest temperatures, which can be also attributed to heat dissipation due to convection cooling. In this context, the temperature distribution can be observed in Fig. 3a, which shows the thermographs of the maximum temperature reached by the different nanocomposites during the thermoelectrical characterization tests. This test allows comparing the homogeneity in heating (shown in Fig. 3b) when using electrically conductive nanocomposites [34]. Here, the MWCNT reinforced nanocomposites present the highest homogeneity, followed by the DWCNT and SWCNT reinforced ones. This behavior can be ascribed to the aspect ratio of the different CNT types since a higher aspect ratio may induce a higher entanglement of the CNTs, leading to a poor dispersion. In this regard, Fig. 3c shows FEG-SEM micrographs of the nanocomposites containing 0.750 wt% of CNTs, where the specimens containing SWCNTs and DWCNTs, respectively, showed a higher CNT entanglement due to their high aspect ratio, whereas the MWCNT reinforced ones showed a much better dispersion of the nanoreinforcement, which leads to a higher homogeneity in heating.

Adding the CNTs in a higher content could enhance the dispersion of the nanoparticles, especially for the CNTs presenting high aspect ratios, due to the higher shear forces applied during the calendering process [33]. In this context, the 0.100 wt% MWCNT and DWCNT reinforced nanocomposites showed an overall suitable Joule heating behavior since these CNT types and contents present both a high temperature-voltage ratio and a high homogeneity in the temperature distribution.

3.2. Water uptake characterization

Fig. 4 shows the water uptake tests for nanocomposites containing MWCNT (Fig. 4a), DWCNT (Fig. 4b), and SWCNT (Fig. 4c) as a function of nanoreinforcement content and time.

Here, the water uptake increases for all nanocomposites until reaching a plateau (M_∞) around 18–20 days. It is worth noting the lower water uptake shown by all the specimens in comparison to similar materials [35]. Furthermore, the increase in CNT content increases the initial uptake rate (slope in the linear region, m). However, the higher the CNT content, the lower the final water uptake they present, regardless of the CNT type. This fact can be explained since the increase

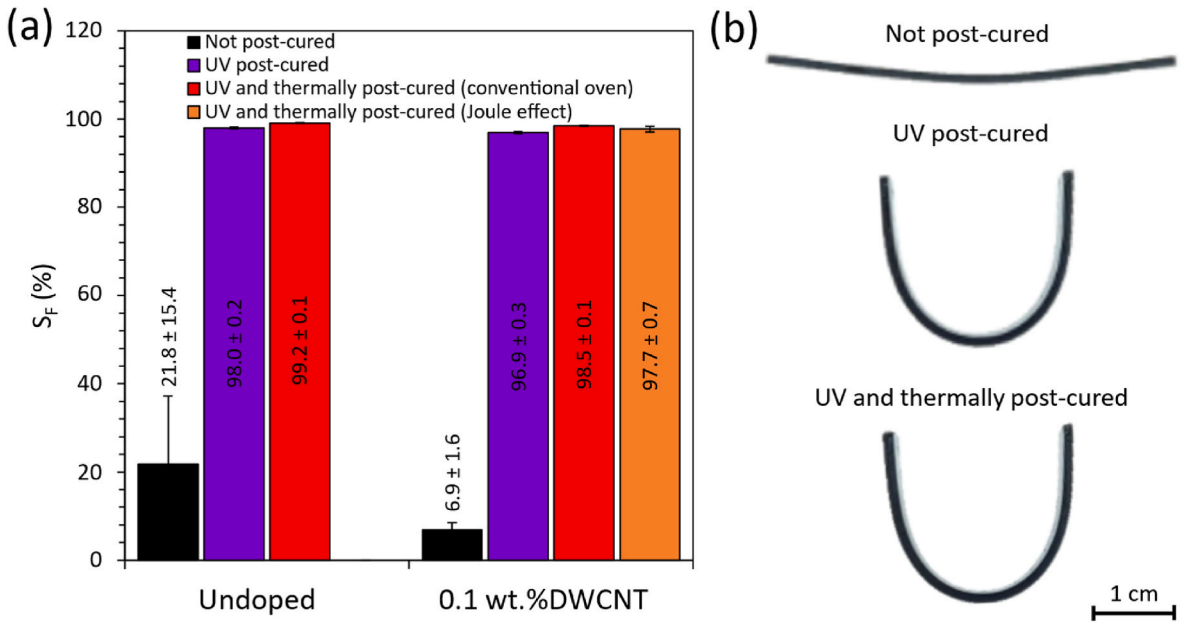

Fig. 7. (a) Shape fixity ratio, S_F, as a function of the post-curing treatment and (b) example of the fixed angles as a function of the post-curing treatment for the 0.1 wt % DWCNT reinforced specimens.

in the CNT content may increase the number of available channels for the water to diffuse into the specimen. This increase in the nanofiller content may also lead to a lower cross-link density due to the UV-shielding effect [33] and steric hindrance [36], resulting in a higher uptake rate in the initial stages. Nevertheless, when the water uptake stabilizes, the increase in the CNT content induces a lower overall water uptake, which can be ascribed to the hydrophobicity of carbon nanofillers [37].

More specifically, the specimen that showed the lowest M_∞ was the one containing 0.1 wt% of DWCNTs, but similar results were obtained regardless of the CNT type. More information on this test can be found in Table S1.

On the other hand, the mechanical properties before and after the water uptake tests for the two conditions that showed the best results in terms of Joule heating, i.e. MWCNT and DWCNT reinforced nanocomposites in 0.1 wt%, were analyzed and compared to the undoped resin by means of DMTA (Fig. 5).

Here, a lower drop in the mechanical properties due to the water uptake is observed for the doped nanocomposites with regard to the undoped resin, which is related to their lower overall water uptake, as previously explained. Moreover, it is important to highlight that, according to the results of the water uptake tests, the hydrothermally aged specimens containing CNTs showed a lower drop in E′ than the undoped specimens with regard to the specimens that were not hydrothermally aged. More specifically, the 0.1 wt%DWCNT reinforced nanocomposites showed the lowest drop in the storage modulus (at 40 °C, the drop in E' of the undoped, 0.1 wt%MWCNT, and 0.1 wt%DWCNT reinforced specimens was 46, 16, and 12 %, respectively).

The aforementioned results evince that the developed nanocomposites can minimize the negative effects of hydrothermal aging with regard to the undoped formulation, proving their suitability to be used in high-humidity environments.

Considering that the best overall results of both the water uptake and the thermoelectrical tests were obtained for the 0.1 wt% DWCNT doped nanocomposites, this CNT type and content was selected as the optimum for the proposed application.

3.3. Thermomechanical behavior

The analysis of the curing degree, carried out by DMTA, is shown in Fig. 6. More specifically, Fig. 6a and b shows the storage modulus (E′) and the T_g (obtained by the tan δ peak), respectively, of the undoped specimens as a function of the post-curing treatment. Here, an increase in both E′ and T_g was induced when performing the UV post-curing stage with regard to the specimen without post-curing, and even increasing when performing the thermal post-curing stage after the UV one. This behavior can be attributed to the higher cross-link density achieved during the post-curing stages since after the 3D printing stage, especially in vat photopolymerization technologies, there are residual reactive species able to react in further curing stages, making the UV post-curing stage practically mandatory [38]. The fact that both the E′ and T_g increase when performing the thermal post-curing treatment suggests that the photocurable system used in this study presents sequential dual curing capabilities due to the presence of radical and thermal radical photoinitiators [39,40]. It is important to point out that the increase in the E' of the non-post-cured specimen above 150 °C is related to the thermal post-curing of the specimen that occurred during the DMTA. Moreover, the non-post-cured specimens showed two different peaks in the tan δ plot, which convolute in one when performing the subsequent post-curing stages. This could be due to the presence of two different monomers in the commercial resin, being the one with the lower T_g more reactive during the post-curing stages, whereas the one with the higher T_g more reactive during the initial UV curing carried out during printing.

Similar results in terms of E′ and glass transition temperature were obtained for the 0.1 wt% DWCNT reinforced nanocomposites, as shown in Fig. 6c and d, respectively. However, when analyzing the results in detail, the E′ of the 0.1 DWCNT doped specimen without post-curing treatment shows a lower E′ in the glassy state and T_g with regard to the undoped specimen. This can be caused by the UV shielding effect of the carbon nanoparticles, since their black color promotes the absorbance of the UV radiation, hindering the photopolymerization process [32,41]. Nevertheless, as can be seen in Fig. 6, the subsequent post-curing stages allow to obtain similar (with the UV post-curing) or even better (with the UV and thermal post-curing) results in terms of E' with regard to the undoped specimens due to the increase in the cross-link density and the effective reinforcement of CNTs.

Additionally, it is worth highlighting the effectiveness of the thermal post-curing carried out by the Joule effect with regard to the one carried out in the conventional oven. In this sense, the E' and T_g are similar, but

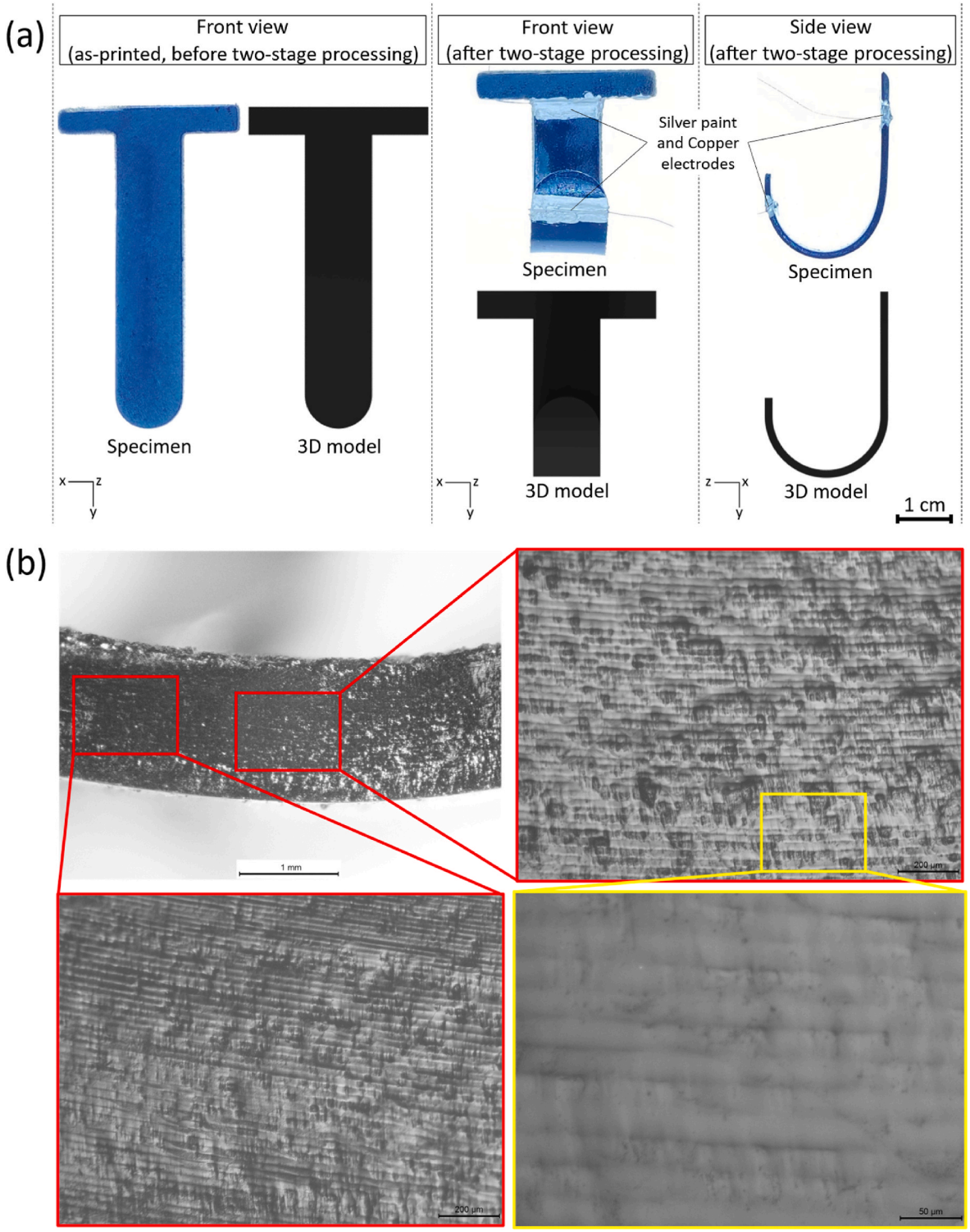

Fig. 8. (a) Front view of the as-printed specimen, before the two-stage processing, and final hook-like shape (front and side view) after performing the subsequent UV and Joule effect thermal post-curing stages. (b) Micrographs of the curved region of the specimen.

slightly lower in the case of the specimens post-cured by the Joule effect, which can be explained by the heterogeneity in heating caused by the presence of CNT aggregates, as previously mentioned, whereas the convectional heating in the oven is more homogeneous.

It is important to point out that this is not the highest curing degree that the specimens can achieve since the T_g increases when performing a second scan in the DMTA (Fig. S1). Nevertheless, the proposed post-curing stages are suitable enough for our purpose, since the specimens are in the glassy plateau at room temperature, which means that the fixed shape is expected to be quite stable. Moreover, an excessive curing degree could lead to a worsening of mechanical properties [42].

3.4. Shape fixity characterization

The shape fixity ratios of the specimens as a function of the post-curing treatment are shown in Fig. 7a. Here, as expected, a very low

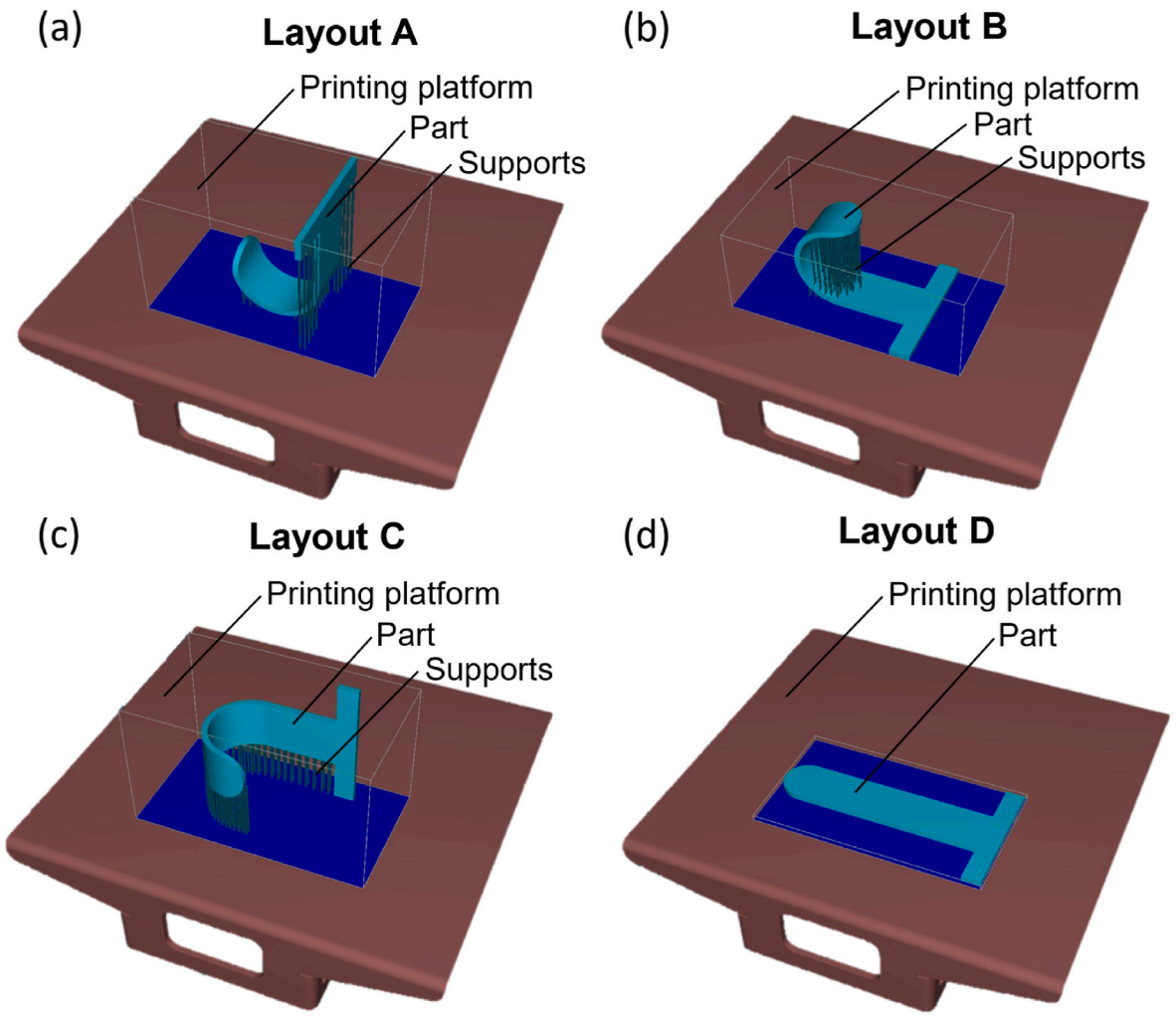

Fig. 9. (a), (b), and (c) 3D Printing layouts (Layouts A, B, and C, respectively) for directly obtaining the proposed hook. (d) 3D printing layout for obtaining the proposed hook via the two-stage processing method (Layout D).

S_F is observed for the specimens without any post-curing treatment. However, the S_F significantly increases when performing the UV post-curing treatment (up to 97–98 %), since the cross-link density increases when the specimen is kept under the applied load to fix the desired shape. In this regard, the newly formed cross-link points when the specimen is set into its desired shape prevent the specimen from recovering its original flat shape. Moreover, the S_F slightly increases when adding the thermal post-curing treatment (up to around 99 %) due to the same reason above mentioned. Furthermore, the thermal post-curing is carried out at a temperature above the T_g, enabling the relaxation of the polymer network thus reducing the residual stress present in the polymer chains caused when bending the specimen after 3D-printing it. An example of the fixed angles as a function of the post-curing treatment for the 0.1 wt% DWCNT reinforced specimens are shown in Fig. 7b.

Furthermore, the effectiveness of the thermal post-curing by Joule heating is evinced since it allows reaching similar shape fixity ratios with regard to the one carried out in the conventional oven. Despite the S_F reached by Joule heating is slightly lower than the one achieved with the conventional oven (97.7 % instead of 98.5 %), the values are high enough to consider using this post-curing method since the energy consumption of the conventional oven (around 750 W) is way higher than the one needed by the Joule effect treatment (around 1 W). In addition, the time needed to reach the desired temperature is in the order of seconds by Joule heating, whereas it is in the order of minutes when using a conventional oven.

When analyzing the effect of the CNTs, the S_F was slightly lower for each tested condition with regard to the undoped specimens. This behavior can be ascribed to the UV shielding effect caused by CNTs, hindering the photocuring reaction and, thus, reducing the cross-link density [43]. Nevertheless, the S_F values are quite similar when performing the UV and thermal post-curing stages, which means that the selected post-curing treatment suitably mitigates the possible negative effect of the UV shielding caused by the nanoreinforcement.

In summary, all the mentioned results related to S_F are in total agreement with the ones obtained in the curing degree tests, since the higher the T_g, the higher the cross-link density and, thus, the more stable the shape is when removing the applied force after the post-curing stages. In this context, the thermal post-curing treatment slightly increases the S_F with regard to the UV post-curing. However, it is important to point out the significant effect that the thermal post-curing treatment has on the T_g and E', as previously explained.

3.5. *Proof of concept*

To evaluate the printing time and material waste savings of the proposed two-stage procedure, a hook was designed and used as an example. Fig. 8a shows the two-stage process carried out with the hook from the flat as-printed shape to the final hook-like shape by initially bending the part, followed by the subsequent UV and thermal post-

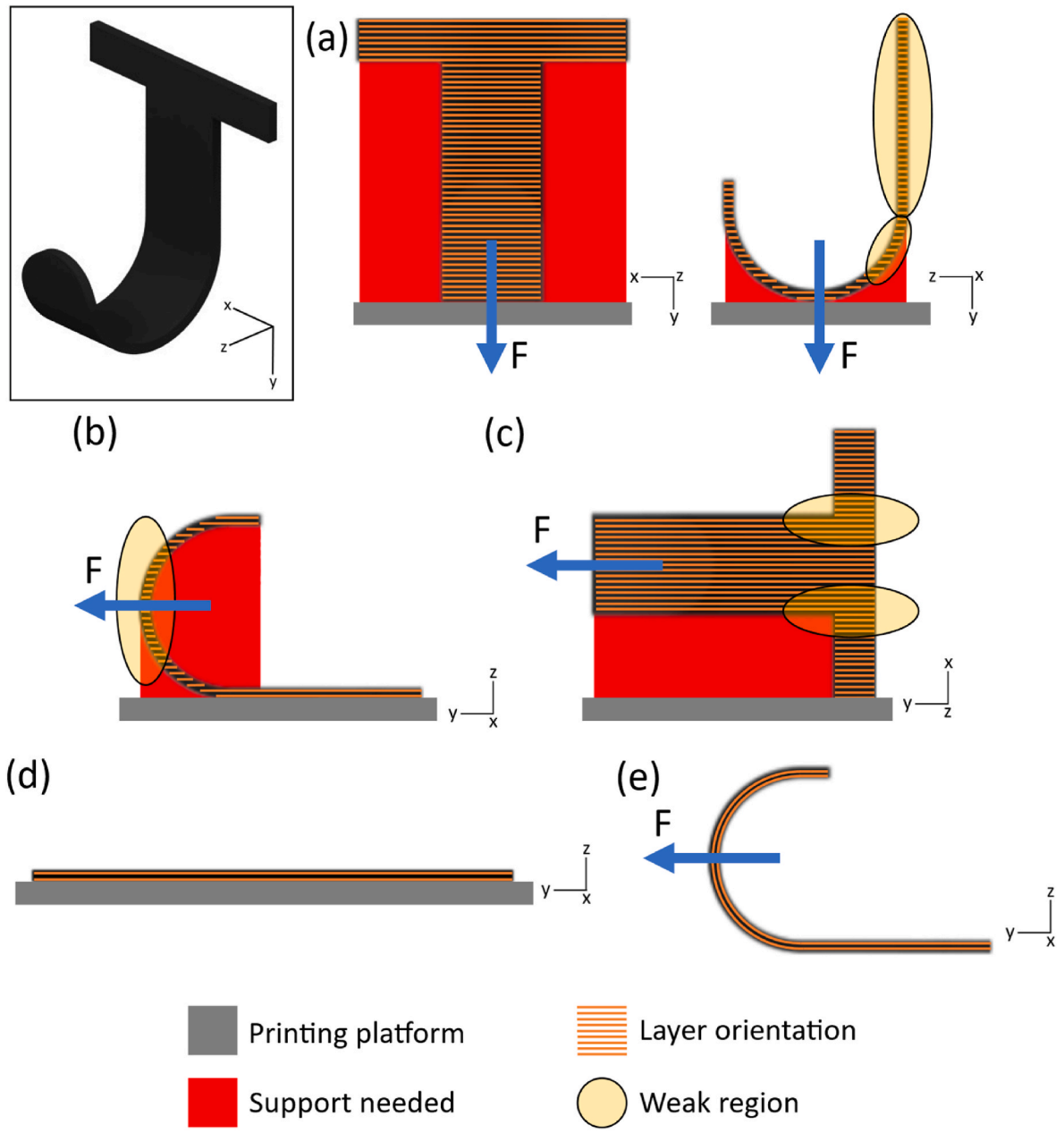

Fig. 10. (a), (b) and (c) analysis of the 3D Printing layouts (Layouts A, B, and C, respectively) for directly obtaining the proposed hook, (d) analysis of the 3D Printing layout (Layout D) for obtaining the proposed hook via the two-stage processing method.

Table 2
3D Printing time, number of layers, material volume, and reduction percent of the printing time and material volume when using the two-stage processing method with regard to 3D printing the specimen directly on its final geometry using the different layouts proposed in Fig. 9.

3D printing layout		Printing time (min)	No. Layers	Material volume (ml)	% reduction with regard to Layout D	
					Printing time	Material volume
Conventional DLP	Layout A	299	1106	1.25	95	15
	Layout B	201	733	1.29	93	18
	Layout C	291	1066	1.28	95	17
Two-Stage processing	Layout D	15	46	1.06	–	–

curing stages. Here, it can be observed once again the high S_F (around 100 %) showed by the developed nanocomposites due to the effective dual curing treatment.

Furthermore, Fig. 8b shows micrographs taken from the curved region of the specimen after the two-stage process. Here, the typical layered structure of 3D-printed parts can be observed. In addition, no delamination between layers were observed after carrying out the two-stage process, proving that the proposed method does not induce any damage to the part.

In this context, the proposed two-stage processing method is

compared in terms of printing time and material waste with regard to directly 3D printing the final shape. Fig. 9 shows the different layout setups used for this comparison. Here, Fig. 9a, b, and 9c show three different printing layouts for directly obtaining the final part, whereas Fig. 9d shows the proposed 3D printing layout for the two-stage processing method. It is important to point out the need for using supports in the cantilever regions of the part, which can be seen in Layouts A, B, and C. As previously explained, no supports are needed when printing flat specimens (Layout D). In this regard, Fig. 10 provides a deeper analysis of the proposed layouts, showing the regions where support structures are needed, as well as the layer orientation and direction of the applied load when in service for every case, which will be discussed further.

Furthermore, Table 2 shows the results of the comparison analysis of the aforementioned layouts carried out using the B9Creator software, showing the printing time, the number of layers, and the material volume needed for printing the proposed layouts, where the reduction of printing time and material waste can be obtained for the two-stage processing method with regard to the different proposed conventional layouts.

Analyzing the results in detail, the printing time of the flat part (Layout D) was just 15 min due to the low amount of printed layers (46 layers), whereas the printing time needed for the parts directly obtained on the final shape (Layouts A, B, and C) ranged from 201 to 299 min (733–1106 layers). Moreover, the material volume needed to print these parts was just 1.06 ml for the flat part since no support structures were needed, whereas the material volume ranged from 1.25 to 1.29 ml for the parts directly printed on its final shape due to the material used for the supports.

Therefore, an average reduction of the printing time of 94.3 %, and an average reduction of 16.7 % was obtained when using the two-stage processing strategy with regard to using the conventional DLP method for the proposed hook.

It is important to point out that the printing time and material waste savings highly depend on the desired final geometry. Nevertheless, the proof-of-concept shown in this work evinced that this simple method can be extremely useful in some cases.

Furthermore, there is an additional possible advantage of the proposed two-stage method related to the reorientation of the printed layers during the process, which is shown in the proposed proof-of-concept. As previously mentioned, Fig. 10 analyzes the proposed printing layouts, including the layer orientation and the direction of the applied load when in service. Here, weak regions are observed in every printing condition when trying to directly obtain the final part (Layouts A, B, and C). This behavior can be ascribed to the anisotropy of the printed parts due to their layered structure [11], showing the Layout A weak regions (highlighted in yellow) where the layers are parallel to bending loads and perpendicular to tensile ones, whereas the Layouts B and C show weak regions where the layers are parallel to the bending loads. In this regard, the hook obtained using the two-stage processing method does not present weak regions when in service (see Fig. 10e) due to the reorientation of the printed layers when fixing the final shape through the sequential UV and thermal post-curing stages.

These excellent results evince not only the suitability of the proposed two-stage processing method for significantly reducing the printing time and the material waste, but also the possibility to enhance the mechanical properties of the 3D printed parts by the reorientation of the printed layers.

4. Conclusions

In this research work, a simple method to minimize the manufacturing time and the material waste during 3D printing, based on a two-stage processing strategy has been successfully carried out. This technique consists of printing a flat specimen, which may considerably reduce the printing time and no supports are needed, obtaining a partially cured specimen. Then, it is swiftly bent into the desired shape, and subsequent UV and thermal post-curing treatments are carried out to increase the cross-link density and thus fix the desired shape.

This method has allowed obtaining an approximately 30 × 30 × 20 mm^3 size proof-of-concept hook by DLP 3D printing technology with an average reduction in the manufacturing time of 94.3 % and avoiding the use of 16.7 % supporting material on average with regard to 3D printing the hook directly on its final desired shape. Additionally, this part has been manufactured containing 0.1 wt% of DWCNTs, which has been optimized as the weight fraction and CNT type suitable for heating by Joule effect, and also showing the least water uptake, thus inducing a lower loss of mechanical properties. The proposed Joule effect heating approach has allowed to fix the part in a bent shape without using any external heating device, such as a conventional oven, which is considerably more energy consuming (750 W against around 1 W), to perform the thermal post-curing stage. Moreover, the shape fixity ratio obtained when applying the two-stage processing method was extremely high (>97.7 %), allowing to perfectly adopt the geometry of the final desired shape.

Furthermore, the proposed method allows the optimization of the mechanical properties of the 3D printed parts when in service due to the rearrangement of the layer orientation when fixing the final shape by applying the subsequent UV and thermal post-curing stages.

In this context, the excellent results obtained using the proposed two-stage processing strategy endorse this method as a real alternative to enhance the efficiency and sustainability of the 3D printing process, being able to produce complex geometry parts saving energy, material waste, and manufacturing time, as well as optimizing the mechanical properties when needed.

Data availability

The raw/processed data required to reproduce these findings cannot be shared at this time as the data also forms part of an ongoing study.

Declaration of competing interest

The authors declare that they have no known competing financial interests or personal relationships that could have appeared to influence the work reported in this paper.

Acknowledgements

The authors acknowledge the financial support received from the Agencia Estatal de Investigación of Spanish Government [PID2022-138496OB-I00 and TED2021-131102B–C21].

Appendix A. Supplementary data

Supplementary data to this article can be found online at https://doi.org/10.1016/j.jmrt.2024.02.018.

References

[1] Dilberoglu UM, Gharehpapagh B, Yaman U, Dolen M. The role of additive manufacturing in the era of industry 4.0. Procedia Manuf 2017;11:545–54. https://doi.org/10.1016/j.promfg.2017.07.148.

[2] Haleem A, Javaid M. Additive manufacturing applications in industry 4.0: a review. Journal of Industrial Integration and Management 2019;4:1930001. https://doi.org/10.1142/s2424862219300011.

[3] Xiang D, Zhang Z, Wu Y, Shen J, Harkin-Jones E, Li Z, et al. 3D-Printed flexible piezoresistive sensors for stretching and out-of-plane forces. Macromol Mater Eng 2021;306:2100437. https://doi.org/10.1002/mame.202100437.

[4] Achillas Ch, Aidonis D, Iakovou E, Thymianidis M, Tzetzis D. A methodological framework for the inclusion of modern additive manufacturing into the production portfolio of a focused factory. J Manuf Syst 2015;37:328–39. https://doi.org/10.1016/j.jmsy.2014.07.014.

[5] Lacroix R, Seifert RW, Timonina-Farkas A. Benefiting from additive manufacturing for mass customization across the product life cycle. Operations Research Perspectives 2021;8:100201. https://doi.org/10.1016/j.orp.2021.100201.

[6] Ngo TD, Kashani A, Imbalzano G, Nguyen KTQ, Hui D. Additive manufacturing (3D printing): a review of materials , methods , applications and challenges. Composites Part B 2018;143:172–96. https://doi.org/10.1016/j.compositesb.2018.02.012.

[7] Conner BP, Manogharan GP, Martof AN, Rodomsky LM, Rodomsky CM, Jordan DC, et al. Making sense of 3-D printing: creating a map of additive manufacturing products and services. Addit Manuf 2014;1–4:64–76. https://doi.org/10.1016/j.addma.2014.08.005.

[8] Gibson I, Rosen D, Stucker B, Khorasani M. Additive manufacturing technologies. third ed. Cham, Switzerland: Springer; 2021.

[9] Savolainen J, Collan M. How additive manufacturing technology changes business models? – Review of literature. Addit Manuf 2020;32:101070. https://doi.org/10.1016/j.addma.2020.101070.

[10] Attaran M. The rise of 3-D printing: the advantages of additive manufacturing over traditional manufacturing. Bus Horiz 2017;60:677–88. https://doi.org/10.1016/j.bushor.2017.05.011.

[11] Redwood B, Schöffer F, Garret B. The 3D printing handbook. first ed. Amsterdam, Netherlands: 3D Hubs B.V.; 2017.

[12] Hu K, Jin S, Wang CCL. Support slimming for single material based additive manufacturing. Comput Aided Des 2015;65:1–10. https://doi.org/10.1016/j.cad.2015.03.001.

[13] Xu Y, Wang Z, Gong S, Chen Y. Reusable support for additive manufacturing. Addit Manuf 2021;39:101840. https://doi.org/10.1016/j.addma.2021.101840.

[14] Fernández-Francos X, Konuray AO, Belmonte A, de La Flor S, Serra À, Ramis X. Sequential curing of off-stoichiometric thiol-epoxy thermosets with a custom-tailored structure. Polym Chem 2016;7:2280–90. https://doi.org/10.1039/c6py00099a.

[15] Colorado HA, Velásquez EIG, Monteiro SN. Sustainability of additive manufacturing: the circular economy of materials and environmental perspectives. J Mater Res Technol 2020;9:8221–34. https://doi.org/10.1016/j.jmrt.2020.04.062.

[16] Kuang X, Zhao Z, Chen K, Fang D, Kang G, Qi HJ. High-speed 3D printing of high-performance thermosetting polymers via two-stage curing. Macromol Rapid Commun 2018;39:1700809. https://doi.org/10.1002/marc.201700809.

[17] Lu C, Wang C, Yu J, Wang J, Chu F. Two-step 3 D-printing approach toward sustainable, repairable, fluorescent shape-memory thermosets derived from cellulose and rosin. ChemSusChem 2020;13:893–902. https://doi.org/10.1002/cssc.201902191.

[18] Fantino E, Chiappone A, Roppolo I, Manfredi D, Bongiovanni R, Pirri CF, et al. 3D printing of conductive complex structures with in situ generation of silver nanoparticles. Adv Mater 2016;16:3712–7. https://doi.org/10.1002/adma.201505109.

[19] Zhang B, Serjouei A, Zhang YF, Wu J, Li H, Wang D, et al. Dual-stage thermosetting photopolymers for advanced manufacturing. Chem Eng J 2021;411:128466. https://doi.org/10.1016/j.cej.2021.128466.

[20] Wang J, Khan M, Hussain A, Khan I, Nawaz A, Ragab AH, et al. Carbon foam composites containing carbon nanotubes and graphene oxide as additives for enhanced mechanical, thermal, electrical and catalytic properties. J Mater Res Technol 2023;24:608–22. https://doi.org/10.1016/j.jmrt.2023.03.056.

[21] Sharma S, Verma A, Rangappa SM, Siengchin S, Ogata S. Recent progressive developments in conductive-fillers based polymer nanocomposites (CFPNC's) and conducting polymeric nanocomposites (CPNC's) for multifaceted sensing applications. J Mater Res Technol 2023;26:5921–74. https://doi.org/10.1016/j.jmrt.2023.08.300.

[22] Xiang D, Zhang X, Li Y, Harkin-jones E, Zheng Y, Wang L, et al. Enhanced performance of 3D printed highly elastic strain sensors of carbon nanotube/thermoplastic polyurethane nanocomposites via non-covalent interactions. Composites Part B 2019;176:107250. https://doi.org/10.1016/j.compositesb.2019.107250.

[23] Xiang D, Zhang Z, Han Z, Zhang X, Zhou Z, Zhang J, et al. Effects of non-covalent interactions on the properties of 3D printed flexible piezoresistive strain sensors of conductive polymer composites. Compos Interfac 2020;28:577–91. https://doi.org/10.1080/09276440.2020.1794479.

[24] Cortés A, Sánchez-Romate XF, Jiménez-Suárez A, Campo M, Prolongo MG, Ureña A, et al. 3D printed anti-icing and de-icing system based on CNT/GNP doped epoxy composites with self-curing and structural health monitoring capabilities. Smart Mater Struct 2021;30:025016. https://doi.org/10.1088/1361-665X/abd343.

[25] Prolongo SG, Díaz-Maroto CG, Jiménez-Suárez A. Electroactive shaping and shape memory of sequential dual-cured off-stoichiometric epoxy/CNT composites. J Mater Res Technol 2021;15:2970–81. https://doi.org/10.1016/j.jmrt.2021.09.102.

[26] Haddar M, Ben Slim Y, Koubaa S. Mechanical and water absorption behavior of thermoset matrices reinforced with natural fiber. Polym Compos 2022;43:3481–95. https://doi.org/10.1002/pc.26630.

[27] Visco AM, Campo N, Cianciafara P. Comparison of seawater absorption properties of thermoset resins based composites. Composer Part A Appl Sci Manuf 2011;42:123–30. https://doi.org/10.1016/j.compositesa.2010.10.009.

[28] Al-Haj Husain N, dent med, Feilzer AJ, Kleverlaan CJ, Abou-Ayash S, Özcan M. Effect of hydrothermal aging on the microhardness of high-and low-viscosity conventional and additively manufactured polymers. J Prosthet Dent 2022;128:822.e1–9.

[29] Jockusch J, Özcan M. Additive manufacturing of dental polymers: an overview on processes, materials and applications. Dent Mater J 2020;39:345–54. https://doi.org/10.4012/dmj.2019-123.

[30] Jiménez-Suárez A, Campo M, Sánchez M, Romón C, Ureña A. Influence of the functionalization of carbon nanotubes on calendering dispersion effectiveness in a low viscosity resin for VARIM processes. Compos B Eng 2012;43:3482–90. https://doi.org/10.1016/j.compositesb.2011.12.009.

[31] Schneider J, Kumar S. Comparative performance evaluation of microarchitected lattices processed via SLS, MJ, and DLP 3D printing methods: experimental investigation and modelling. J Mater Res Technol 2023;26:7182–98. https://doi.org/10.1016/j.jmrt.2023.09.061.

[32] Cortés A, Sánchez-Romate XF, Jiménez-Suárez A, Campo M, Ureña A, Prolongo SG. Mechanical and strain-sensing capabilities of carbon nanotube reinforced composites by digital light processing 3D printing technology. Polymers 2020;12:975. https://doi.org/10.3390/POLYM12040975.

[33] Cortés A, Sánchez-Romate XF, Jiménez-Suárez A, Campo M, Esmaeili A, Sbarufatti C, et al. Complex geometry strain sensors based on 3D printed nanocomposites: spring, three-column device and footstep-sensing platform. Nanomaterials 2021;11:1106. https://doi.org/10.3390/nano11051106.

[34] Cortés A, Cosola A, Sangermano M, Campo M, González Prolongo S, Pirri CF, et al. DLP 4D-printing of remotely, modularly, and selectively controllable shape memory polymer nanocomposites embedding carbon nanotubes. Adv Funct Mater 2021;31:2106774. https://doi.org/10.1002/adfm.202106774.

[35] Arribas C, Prolongo MG, Sánchez-Cabezudo M, Moriche R, Prolongo SG. Hydrothermal ageing of graphene/carbon nanotubes/epoxy hybrid nanocomposites. Polym Degrad Stabil 2019;170:109003. https://doi.org/10.1016/j.polymdegradstab.2019.109003.

[36] Sánchez-Romate XF, Martín J, Jiménez-Suárez A, Prolongo SG, Ureña A. Mechanical and strain sensing properties of carbon nanotube reinforced epoxy/poly(caprolactone) blends. Polymer 2020;190:122236. https://doi.org/10.1016/j.polymer.2020.122236.

[37] Prolongo SG, Gude MR, Ureña A. Water uptake of epoxy composites reinforced with carbon nanofillers. Composer Part A Appl Sci Manuf 2012;43:2169–75. https://doi.org/10.1016/j.compositesa.2012.07.014.

[38] Šťaffová M, Ondreáš F, Svatík J, Zbončák M, Jančář J, Lepcio P. 3D printing and post-curing optimization of photopolymerized structures: basic concepts and effective tools for improved thermomechanical properties. Polym Test 2022;108:107499. https://doi.org/10.1016/j.polymertesting.2022.107499.

[39] Fernández-Francos X, Konuray O, Ramis X, Serra À, de la Flor S. Enhancement of 3D-printable materials by dual-curing procedures. Materials 2021;14:1–23. https://doi.org/10.3390/ma14010107.

[40] Ramis X, Fernández-Francos X, de la Flor S, Ferrando F, Serra A. Click-based dual-curing thermosets and their applications. Thermosets: structure, Properties, and Applications. second ed. first ed. Amsterdam, Netherlands: Elsevier; 2018. p. 511–41. https://doi.org/10.1016/B978-0-08-101021-1.00016-2.

[41] Gonzalez G, Chiappone A, Roppolo I, Fantino E, Bertana V, Perrucci F, et al. Development of 3D printable formulations containing CNT with enhanced electrical properties. Polymer 2017;109:246–53. https://doi.org/10.1016/j.polymer.2016.12.051.

[42] Taormina G, Sciancalepore C, Messori M, Bondioli F. 3D printing processes for photocurable polymeric materials: technologies , materials , and future trends. J Appl Biomater Funct Mater 2018;16:151–60. https://doi.org/10.1177/2280800018764770.

[43] Cortés A, Aguilar JL, Cosola A, Fernández Sánchez-Romate XX, Jiménez-Suárez A, Sangermano M, et al. 4D-Printed resins and nanocomposites thermally stimulated by conventional heating and IR radiation. ACS Appl Polym Mater 2021;3:5207–15. https://doi.org/10.1021/acsapm.1c00970.